Presented at the 37th European PV Solar Energy Conference and Exhibition, 7-11 September 2020

THE CRYSTAL GROWTH EXPLORER: REAL-TIME NAVIGABLE 3D VISUALIZATION OF SILICON GRAINS AND DEFECT RELATED DATA IN CAST-MONO AND MULTICRYSTALLINE BRICKS

J. Schönauer[1], M. Demant[1], T. Trötschler[1], A. S. Kovvali[1], H. Schremmer[2], P. Krenckel[1], S. Riepe[1], S. Rein[1]
[1] Fraunhofer Institute for Solar Energy Systems ISE, Heidenhofstr. 2, 79110 Freiburg i. Br., Germany
[2] Meyer Burger (Germany) GmbH, Aachener Str. 100, 53909 Zülpich, Germany
Phone: +49 761 - 4588 2080; e-mail: jonas.schoenauer@ise.fraunhofer.de

ABSTRACT: Development of novel materials for silicon solar cell production like SMART mono material with functional grain boundaries depends on the human insight and understanding of the structural and dynamic properties of the underlying crystallization process. In this work, we present an analysis and visualization process that allows for comfortable, flexible human exploration and interpretation of various crystallization-related data types ranging from per-wafer photographic images and defect measurements to segmented and 3D-reconstructed grain and defect data, by putting and combining them in a concrete, meaningful, vivid visualization context close to the spatial structure of the actual grown crystal. We address two urgent challenges for smart mono development by combining appropriate data analysis and inspection methods: (1st) analyzing crystal growth characteristics for non-destructive quality inspection and (2nd) investigating defect scenarios for identifying the best crystallization recipes.

Keywords: Crystallization, cast mono, SMART seeding, characterization, visualization, grain, dislocation, data analytics, machine learning

1 INTRODUCTION

The efforts to improve the silicon crystallization process have led to a variety of measured data of different kind, format and origin. Discovering and revealing the hidden structures, phenomena and relations within that data is key for understanding crystallization as a whole and in detail. While humans are capable to quickly identify patterns and track anomalies in visually accessible data, the amount, fragmentation, size and diversity of data arising from brick and wafer inspection makes it difficult to directly discover correlations between the various data points and to understand the root causes of crystallization phenomena observed.

This work addresses the evaluation of mass of data, by presenting an efficient, software-based inspection process for screening, inspection and analysis of the available data via a user-friendly workflow and rich visualizations. We target the following use-cases:

- Quick non-destructive quality inspection from production brick and wafer data
- Investigating crystal and defect growth characteristics for optimizing crystallization recipes
- Detailed analysis of local growth patterns and defect scenarios

1.1 A Data Analysis and Visualization Platform

Our approach combines analysis steps of data-dependent preprocessing with a graphical software tool for data sighting, selection and exploration by the user. It uses image processing and deep neural networks to extract, combine and condense data of inline and offline brick and wafer analysis. Ordered overviews, flexible 2D data compositions as well as dynamic 3D rendering in brick context are then applied to quickly understand a grown crystal structure and its relation to defects.

For quality inspection of crystal growth in cast-mono and multicrystalline bricks, we present 3D reconstruction visualizations of grains and dislocation clusters that can be dynamically explored by the user. For quick feedback, raw measurement data can immediately be used for flexible 2D data overlay and certain 3D perspectives. For the analysis of defect scenarios, combined visualizations of grain and defect data can take place.

The presented image processing and data analysis methods build on top of various related works [1–6], where wafer measurement and data analysis methods have been established, which are now used as input data to interactively visualize the crystallization artefacts in various 2D and 3D perspectives.

While hp-mc silicon grains and dislocation clusters as a whole or as single objects have been tomographically reconstructed and visualized in 3D space before [6–10], we extend and generalize the visualization concept to cast-mono silicon and a range of visualization modes including combined visualization of multiple data types. We further embed those visualizations into an interactive software with a focus on usability on a daily basis, on top of a mostly automated data analytics setup.

1.2 Use-Cases for Crystallization Analysis

For cast-mono bricks, we examine the growth of the monocrystalline region and unwanted grain ingrowth from the crucible edge, as well as the spreading of dislocations within the crystal. For multicrystalline silicon, we observe the interaction of dislocations and grain boundaries in detail.

One particular active topic of interest is the reduction of defects in cast-mono silicon. Dislocation clusters induced by seed plate joints and parasitic grains nucleated at the crucible walls can be successfully controlled with appropriate seeding configurations and SMART stacks [11, 12]. We visualize the effect of functional grain boundaries on dislocation development and parasitical grain growth.

A problem still remaining is the appearance of dislocation structures within the monocrystalline part of cast-mono ingots [13] that have no visible connection to seed plates, grain boundaries, crucible walls or other dislocation clusters. We design a combined data visualization mode that shows a connection between recombination active dislocation clusters appearing inside the mono-crystalline part and PL signal fluctuations in the lower brick regions in combination with inclusions.

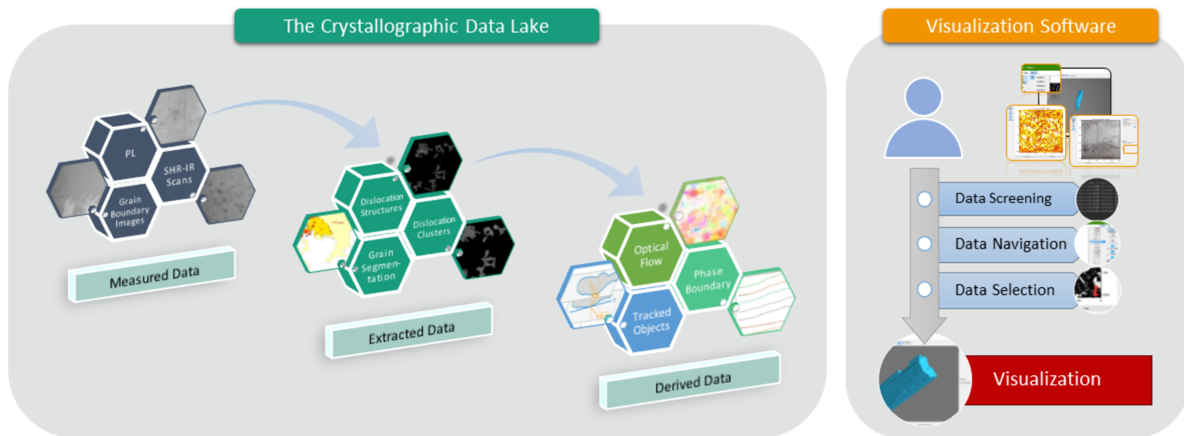

Figure 1: The flow of data from measurement to visualization as described in this paper. **(Left)** The data for visualization originally comes from (i) measured data of different devices such as grain boundary or PL images. (ii) The valuable information such as grain boundary coordinates or dislocation structures is extracted. (iii) Refined, abstract data like 3D tracked grains is computed from the extracted data. **(Right)** All of those data types from different stages are indexed by the visualization software and presented to the user as an organized structure. A visualization of choice is then selected by the user and the respective data is visualized using different 2D or 3D based modes.

2 VISUALIZATION PROCESS

An interactive analysis and visualization tool places special demands on the speed, resource consumption and accessibility of the data processing mechanisms. For this reason, the visualization workflow is split into an extensive, preparative data analysis stage, and a user-faced software optimized for high responsiveness and efficient workflows. The overall process can be roughly divided into three stages:

1. **Advanced Data Analysis**: Electrical and optical data measured on brick and wafer level is acquired and analyzed by image processing and/or machine learning.
2. **Efficient Exploration Pipeline**: The available data is indexed according to metadata by the visualization software. The user chooses a desired brick, visualization type and data type and object of interest, depending on the visualization type.
3. **Optimized Presentation**: The related source data is read, filtered and transformed into an optimized, descriptive, display-friendly format. The grain or defect data is visualized in 2D or 3D in context of the brick. The user can navigate within the visualization and inspect the data of interest.

Figure 1 shows an overview of the general workflow. The various data analysis steps are performed script based after a new experiment took place, whereas the data exploration and presentation steps happen in the visualization software in real-time.

2.1 Data Analysis

For the use-cases described in this paper, the data can be categorized into grain, dislocation or inclusion related data. While we present visualization types specifically tailored to certain questions such as grain growth characterization, the basic procedure can be considered open in terms of the type of data visualized. Every kind of data point which is measured in relation to a specific location in a brick can be organized and visualized in the three-dimensional context of that brick, and be combined with other data belonging to the same brick and location. This applies to most data which are measured at wafer or brick level, as long as the relation to the original brick is known.

From the raw data, we extract information and derive crystallization-related parameters using traditional image processing and machine learning algorithms. All 2D image data is initially aligned to a 1024 x 1024 pixel wafer square.

Grain boundaries and grain segments are extracted from grain boundary images, which combine multiple optical images per wafer with white light illumination from eight different angles [14]. The extraction is done via image segmentation as described in [14], using region-growing with a distance measure created for stacks of optical images. Beforehand, the images are preprocessed with anisotropic diffusion [15] and mean shift filtering for reducing signal noise.

Dislocation lines are extracted from photo-luminescence (PL) images of wafers by classical image processing or deep learning techniques as shown for brick data in [16]. Extracted dislocations are separated from recombination-active grain boundaries as described in [1]. To analyze groups of related dislocations, clusters are built by morphological processing of extracted lines.

Needle and point inclusion coordinates are provided by brick side scans using a super high resolution infrared transmission (SHR-IR) measurement system [17]. The local inclusion density is calculated at creation time of the visualization by 3D bin counting (3D histogram).

Vertical development of grain boundaries and dislocation clusters is modeled by optical flow as in [4, 6], computed from grain boundary images or PL images using variational algorithms [18, 19]. Also deep learning algorithms [20] showed good results. An example for two wafers and the according optical flow field between their grain boundary images is shown in Figure 2. For the visualization of 3D grains, all 2D wafer segments are combined. Therefore, Grain ID maps are created from tracking the grains' segments along brick height with the help of the optical flow field. Likewise, dislocation cluster ID maps are calculated from optical flow and extracted 2D clusters.

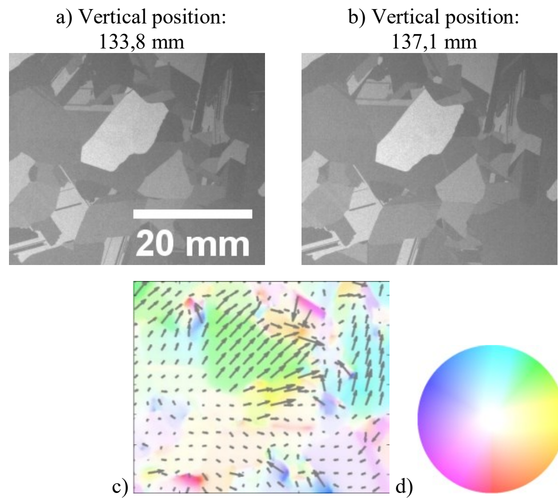

Figure 2: a), b) Grain boundary images of two neighbouring wafers of an hp-mc-Si brick. c) The optical flow from a) to b) is visualized by vector arrows. The image shows the same region as in a). d) The circle color code is another way to visualize the vector direction (angle / hue) and magnitude (radius / saturation).

2.2 Exploration Pipeline

For an interactive evaluation of large amounts of data, various challenges arise: i) To process the data without delay for the user in face of limited resources of computing power, memory capacity, ii) to offer suitable, user-friendly controls to survey and access this pool of data, and iii) to find perspectives and views that unveil the complex physical relations within the data in a visually comprehensible manner. Therefore, the visualization concept was optimized to increase reactivity, flexibility and usability of the toolkit throughout the whole workflow:

1. The graphical visualization software automatically scans and indexes the available data. The attribution to a certain brick and ingot happens according to configurable naming and file format schemes.

2. The user may browse the available data organized per brick (data screening) use tailored, easy-to-use selection mechanisms to decide on the desired data and visualization type (data selection). For example, for displaying the 3D reconstructed model of a specific grain of interest, the user screens the available grain data in the grain selection view shown in Figure 3.

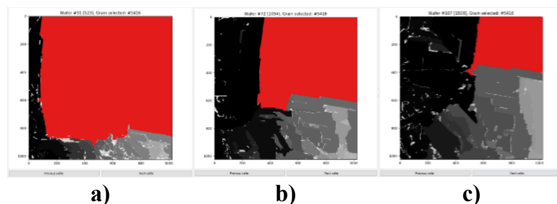

Figure 3: One-click selection mechanism to focus on interesting grains in wafer data screening view. The example show a wafer in the **a)** low **b)** middle **c)** upper third of a cast-mono brick with selected main grain tracked and highlighted (red) over multiple wafers.

A grain of interested is selected with a mouse-click. The grain is internally automatically identified according to the precomputed grain ID maps, and subsequently highlighted in the view for all the wafers of the brick. Once the user has decided, a 3D visualization for the currently selected grain can be computed on demand.

3. The actual data reading procedures and processing steps are carried out at the latest possible time and limited to the data required for the respective visualization (e.g. wafer by wafer). The technical selection of the data sources, file paths and processing steps necessary for browsing or computing the requested visualization is carried out behind the scenes without user intervention.

4. Raw data is read directly from the respective measurement directories, if possible in the original format, so that an initial evaluation of measured data can take place immediately after a new experiment. Results of data analysis methods as described in Section 2.1 are read from corresponding result files once they are available.

5. Source data of resource-demanding visualizations, especially 3D tomograms, are transcoded shortly before presentation into a hardware optimized format, for example by coordinate interpolation onto a regular grid and triangulation to a polygon model. Together with the use of established and optimized 3D visualization frameworks [21, 22] this allows for a fluid presentation and real-time navigability of the 3D scene.

2.3 Visualization Modes

Based on current crystallographic questions, visualization modes were designed and implemented, each of which offers its own perspective on the processes inside the brick.

2D-Wafer-Slices, as shown in the grain selection stage in Figure 3, is a visualization mode that displays two-dimensional data in a structured manner along the height of the brick. Because of the very low computational demands for raw 2D data sources, this is a fast and direct view. In conjunction with intuitive navigation controls, like mouse wheel scrolling, this mode allows for quick and fluid navigation through the available wafer data of a chosen brick. The ability to virtually move through the wafer data of the brick from bottom to top was previously reported as a surprisingly effective means to get an overview of preliminary growth patterns as well as to study single grains and defects [10].

Reconstructed 3D models allow a spatial representation of tomographically reconstructed objects. This visualization provides an overall impression of the shape, size, position and development of individual grains or dislocation clusters.

Virtual 3D sections are virtual sectional planes freely positionable in the 3D brick context for volume data types in perspective or isometric view. This visualization is suitable for the focused analysis of details or internal structures that are otherwise hidden within the opaque 3D reconstruction of the entire object. In isometric view, it is also suitable for determining geometric properties, such as the over-growth angle.

Data overlay visualizations allow the combination of different, compatible data sources in 2D or 3D sectional view. The different data types can be distinguished by using a neutral, grayscale background for one data channel, and a superimposed, colored heat map for the other. By combining them in a common spatial context, correlation and mutual interaction between the data sources can be investigated.

3 CRYSTALLOGRAPHIC INVESTIGATIONS

3.1 Experimental

As part of a larger, recent project at Fraunhofer ISE, an extensive data collection of over 100 000 wafers from more than 500 bricks and measurements on brick and wafer level has been recorded. It contains both cast-mono and high-performance mc-Si (HPM) material, produced with different seeding configurations and crystallization recipes in G2 and G6 format. For the different ingots, bricks have been systematically wafered and measured. The resulting collection of brick wafer data at close intervals is a valuable data source for analysis and 3D reconstruction methods described in this paper.

We apply the data processing and visualization concepts to an exemplary selection of this data and investigate key crystallographic topics of interest by the use of targeted visualizations.

3.2 3D Crystal and Dislocation Cluster Growth

The first crystallographic field of interest shown is the 3D growth shape of grains and dislocation clusters. To allow a detailed insight into those, we chose the straightforward approach of using our presented 3D grain and dislocation cluster reconstruction algorithms (see Section 2) combined with 3D modelling and displaying of the resulting objects.

Figure 4 shows an example of the main grain of a cast mono corner brick. The visualized brick outline allows for a clear impression of the shape and position of the mono grain inside the corner brick. Also the reduction in size induced by parasitic grain growth from the crucible walls can be seen immediately. The 3D scene can be freely rotated, zoomed and translated, which allow for inspection of the whole picture but also to catch small details in the structural growth at the grain boundaries up to the resolution of the source data. The cut-off at the top of the grain is due to a lost 3D connection in the 3D tracking phase (see Section 2), still, most of the grain slices were tracked correctly.

The result of the dislocation cluster reconstruction and 3D modelling are shown in Figure 5. In contrast to the grain visualization example, all the detected dislocation clusters of the whole brick are visualized at once, since the distribution of dislocations is sparse and single clusters can be visually distinguished. Shape, growth direction and expansion of single clusters, as well as the overall dislocation development can be recognized with this visualization.

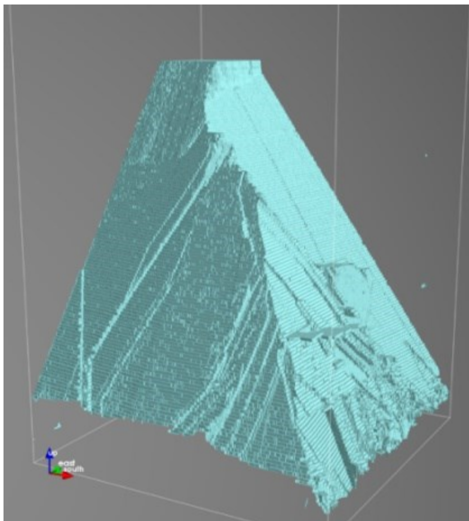

Figure 4: Navigable 3D visualization of a monocrystalline grain of a cast-mono corner brick (with brick outline, the inner corner of the brick being located behind the grain).

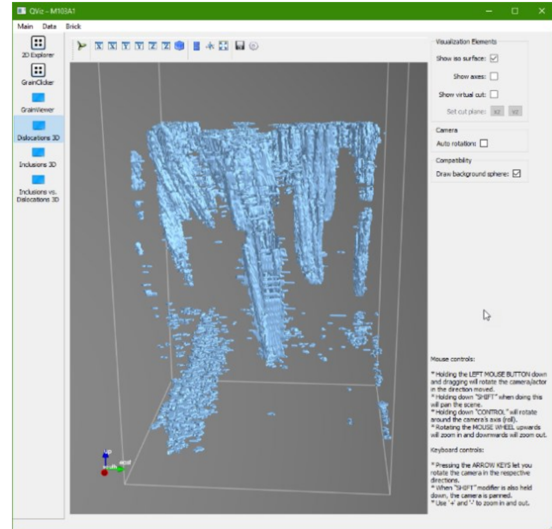

Figure 5: Navigable 3D visualization of a G2 cast-mono corner brick's dislocation clusters with brick outline in the visualization software. The inner corner of the brick is located in the lower right of the figure.

3.3 Grain Structure in HPM Silicon and Interaction with Dislocation Development

In order to investigate the interaction of grain boundaries and dislocations, we use extracted grain boundary data as described in Section 2.1 and visualize it in 2D wafer slice mode. To make the single grains visually distinguishable from each other, a color code is applied that maps the relative area of grain segments to a greyscale value. The interaction with dislocation structures is revealed by overlaying the extracted dislocations onto the 2D image, as seen in Figure 6.

Following the evolvement of single grains from bottom to top of an ingot, characteristic growth phenomena such as grain coarsening can be studied in detail. The influence of fluctuations in the growth process on the grain development can be visualized and evaluated. Also nucleation of new grains or twinning as relevant processes, especially near the ingot edge, can be investigated in correlation to the thermal growth process.

The investigation of the increase or decrease of recombination-active dislocation clusters in relation to the grain structure development has been intensely studied for HPM silicon. A combination of the grain structure information with the positions and densities of dislocation clusters for wafers of different ingot heights have been used to identify specific grain configurations for which the overall amount of dislocation tangles in a specific area diminishes as shown in Figure 7. It could be shown that the reduction of dislocation cluster size over ingot height is mostly induced by the overgrowth of the specific defected grain by a differently oriented grain without dislocation. The dislocation tangles are stopped at the grain boundaries and seem to be "pushed" in front of grains with a non-vertical growth axis.

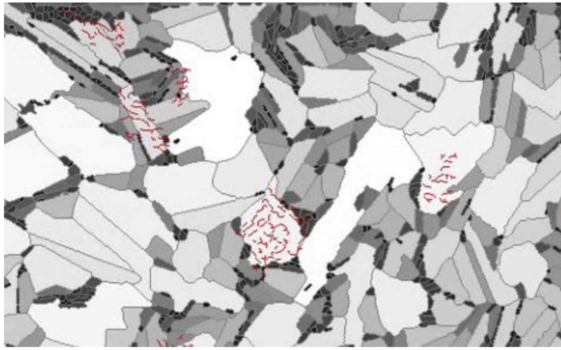

Figure 6: Visualization of grain boundary interaction with dislocations in a HPM wafer, created using extracted grain segments, greyscale color-coded by relative area, overlaid by extracted dislocations.

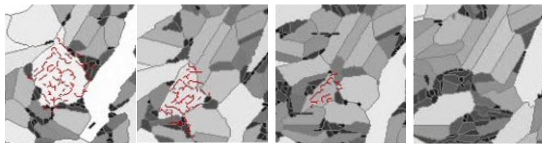

Figure 7: Detail view of a grain in the center of Figure 6. The same cropped region is shown over multiple wafers with raising height in brick.

3.4 Grain Growth and Dislocation Development in Cast-Mono-Silicon

Further development of cast-mono crystals aims for the reduction of dislocations and parasitic grains inside the mono-part of the ingot. For the evaluation and comparison of different seeding configurations and recipes, methods for detailed quality control of the inner brick regions are necessary. We generate such methods by combining defect and grain related data into insightful visualizations.

2D Analysis of SMART Mono-Silicon. Our quality inspection shows the impact of functional grain boundaries induced by the SMART seeding technique. Figure 8 depicts a visualization created by combining PL wafer data with extracted grain boundaries, taken from respective measurements of wafers close to each other in brick height. The example is comparing two cast-mono corner bricks, one without and one with SMART grain boundaries, with the crucible walls being on the left and top side of the image. The samples in the bottom row of Figure 8 originate from the lower part of the brick, where most of the mono grain is still free of differently oriented grains or recombination-active dislocation clusters. In contrast, in the top of the brick, shown in the top row of Figure 8, parasitic grains are covering about three thirds of the wafer area in case of the non-SMART brick. By using SMART stacks, parasitic grain growth could almost be prevented on the left-hand side and greatly reduced on the upper image side, with the mono-grain still being the largest grain on the wafer. In all examples, the grain boundaries introduced by the seed plate joints are visible by the dark lines of the PL signal.

Growth Scenarios. The combined visualization of PL data with grain boundaries allows identifying characteristic behaviors and growth scenarios. In Figure **9**, we investigate a cast-mono brick at the crucible wall. By combining the two measurements, it is revealed, that the ingrowing group of parasitic grains in this example is actually preceded by a front of dislocation clusters.

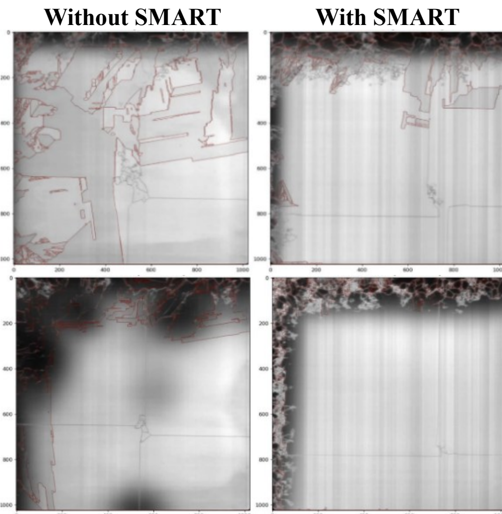

Figure 8: Comparative visualization of PL data with overlaid extracted grain boundaries (red) of two G2 cast-mono corner bricks (left column) without and (right column) with SMART seeding. Samples were taken from (top row) ~130 mm height and (bottom row) ~67 mm height in brick.

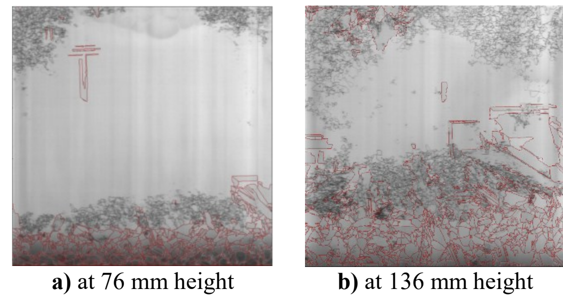

a) at 76 mm height **b)** at 136 mm height

Figure 9: Combination of PL data (gray) with extracted grain boundaries (red) of a cast mono edge brick wafer at different heights in brick (bottom side faces the crucible).

During the observed crystallization process, grains and dislocations develop with the same growth direction and speed, keeping the dislocations ahead.

As in the case of HPM silicon, described in Section 3.3, dislocations can be absorbed by the advancing grain boundaries. However, this is not the case for the monocrystalline region. Since there remain no sinks for dislocations inside the monocrystal to stop the dislocation movement, recombination-active dislocation clusters can multiply and extend further into that region.

3D Reconstruction for SMART Mono-Silicon. We analyze the vertical development of dislocations by means of tomographical PL data in combination with inclusion density data (Figure 10). The visualization of the solid data block resulting from the PL wafer data stack is opened up by virtual cut planes, which allow setting targeted vertical slices through specific dislocation clusters of interest. In the example, the visualized brick is a cast-mono edge brick (crucible facing side on the left) with a SMART stack in the seeding configuration visible in the lower cutting plane. Slicing the data vertically allows to estimate the vertical spreading of the cluster throughout the brick and during the crystallization. In this example slice, the blocking effect of the functional grain boundaries induced by the SMART stack on dislocation growth is clearly visible.

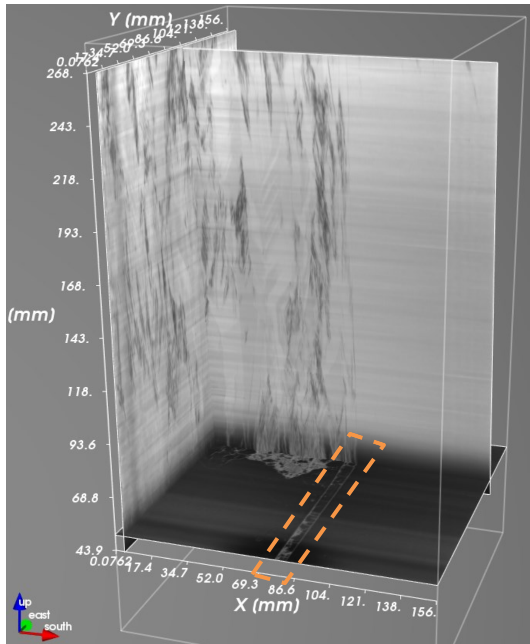

Figure 10: 3D visualization of the PL data of a G6 cast-mono edge brick. The 3D data is accessible via three independent, freely rotatable and movable cutting planes. The crucible facing side is located in the left of the picture. A SMART stack is visible in the bottom cutting plane (orange dashed rectangle), as well as the vertical development of the resulting functional defects in the vertical cutting plane in the back.

3.5 Growth Process Analysis by Combined 3D Visualization

To draw a connection between recombination-active dislocation clusters inside single mono grains and other defects, we combine tomographically stacked raw PL data of affected bricks with 3D inclusion density data. To understand the spatial relations in the local surroundings, we embed the two defect types into a 3D visualization with freely adjustable cutting planes, and align them to the dislocation clusters of interest.

Figure 11 shows the resulting visualization for an affected brick with raw PL data. When the cut plane is aligned with the origin and growth direction of the dislocation cluster, as shown in the example, two things become apparent:

1) The dislocation cluster in focus becomes visible in PL data and starts to spread right above a high inclusion density layer in the brick.

2) Extending the growth direction of the cluster and reversely following it to the bottom of the brick, small dark lines can be spotted in the PL signal below the first high inclusion density layer.

We repeated this visualization method for different dislocation clusters and different bricks. Not for each dislocation cluster those early fine lines could be spotted. If they were found, their exact appearance also varies in terms of visibility, absolute height in brick and height relative to the first high inclusion layer. However, it could still be qualitatively observed, that a high count of early PL fluctuations in general coincides with strong recombination-active dislocation cluster development above high inclusion layers further up in the brick and vice versa.

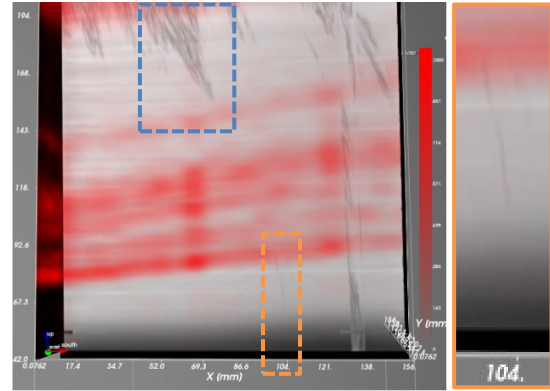

Figure 11: Combined 3D visualization of PL data (grey background) and particle inclusion density (red overlay) of an inner brick of a cast-mono ingot, realized with virtual cut planes. The view is centered towards a vertical cut plane, which has been manually positioned on the apparent origin of the visible dislocation cluster in the top of the brick (blue rectangle), and manually rotated to match its predominant direction of growth. The area marked with the dashed orange rectangle is zoomed in on the right.

This observation is in accordance with other studies looking at the crystallographic properties of the grown monocrystalline region directly above the remaining mono seed. Trempa et al. [23] could reveal dislocation cells in the seed and the monocrystalline region above by selective etching of dislocations. These dislocation cells can grow up to the ingot top and may be transformed into highly recombination-active sub grain boundaries. The visualization method applied here could help to further investigate the correlation between this transformation process and the layers with high inclusion density.

4 DISCUSSION

From a crystallographic perspective, the presented methods offer a valuable insight into a grown crystal structure and facilitate the evaluation of crystallization parameters. Visualizing crystallization data in a 3D brick context opens up the opportunity to interpret crystal growth data with the spatial understanding of the human mind.

For materials with few single grains like cast-mono Silicon, crucial properties like grain structure and dislocation clusters are quickly assessed, for example the shrinkage of the mono-crystalline part, i.e. the grain with seed orientation, with increasing ingot height. The vertical development of the mono-crystalline part yields information on the number of wafers that can undergo a solar cell process designed for monocrystalline material. This turns these visualizations into a valuable, non-destructive feedback method regarding the quality of the mono-cast material, entirely based on inline-compatible wafer measurements.

The vertical development of PL data and extracted dislocations, in conjunction with flexible visualization modes like 3D virtual cut planes with fully configurable position and rotation, reveal where and how well functional grain boundaries have worked. Crystal growers can further draw information from combining the visualization of grain, dislocation and inclusion data. The data overlay mechanism is a simple yet powerful

method to find anomalies, explore hypotheses and discover relationships and growth patterns between different measurement data, for example interactions of grain boundaries with dislocations. In case of recombination-active dislocation clusters inside mono-crystalline parts, the visualization presented in Section 3.5 gives a valuable hint for investigations needed to further improve the cast-mono technology.

Also from a technical and workflow perspective, the implemented software and the data exploration concept turn out as helpful in daily use for controlling and understanding the crystallization process. The interactive 2D wafer data display is a basic yet powerful way of quickly getting an impression of the available data and both the overall data development as well as 2D inspection of detail phenomena. The intuitive selection mechanisms allow for a quick workflow of identifying grains and defects of interest and tracking their development in 2D or 3D view. Due to our data management and the use of optimized render technology, we are able to visualize main grains of mono-cast bricks as well as full brick dislocation clusters in a responsive, live-rendered 3D environment on a standard desktop computer.

Still, work has to be done in the area of more robust tracking algorithms for 3D reconstruction of single objects and robust 2D segmentation. Despite the tracking is good enough to construct objects meaningful to human interpretation, a single miss will result in apparently broken or cut-off grains and clusters, an issue that some of our visualizations suffered from.

5 CONCLUSION

We introduced the "Crystal Growth Explorer", a data visualization toolkit for quickly assessing the inner structure of multicrystalline and cast-mono bricks from brick level and inline-compatible wafer level measurements. It combines extensive data analysis and feature extraction methods (previous work) with a performant, interactive, graphical software for efficient data screening, exploration and inspection. Various real-time 2D and 3D visualization modes, flexible data overlay, intuitive data navigability and a focus on usability allow for both quick feedback as well as structured data analysis.

The following data types have been integrated and visualized:

- 2D grain boundaries and grain segments
- 2D dislocations tangles and clusters
- 3D reconstructed grains
- 3D reconstructed dislocation clusters
- Raw photoluminescence data
- Motion vector fields (optical flow) between grain boundary / PL images of subsequent wafers
- Super-high-resolution IR transmission scans and inclusion density

Use-cases can be found in non-destructive process quality control for industrial production as well as research and development of new materials like cast-mono-Si with SMART functional grain boundaries. In particular, we presented visualizations addressing the following crystallographic topics of interest:

(1) Process control and comparison of seeding configurations effects for cast-mono development.
(2) Interaction of grain boundaries and dislocations in mc-Si.
(3) Showing the spatial effect of functional grain boundaries on dislocation development and parasitic grain growth.
(4) Investigating growth and defect scenarios involving multiple defect types and data sources. Here we could draw a connection between recombination-active dislocation clusters appearing inside the mono-crystalline part of cast-mono bricks, and PL signal fluctuations in the lower brick regions in combination with areas of high inclusions.

ACKNOWLEDGMENT

This work was funded by the German Ministry for Economic Affairs and Energy (BMWi) within the frame of the project "Q-Crystal" (contract number 0324103A).

6 REFERENCES

[1] T. Strauch, M. Demant, P. Krenckel, and Riepe, S., Rein, S., "Grain Boundaries and Dislocations in Si-bricks: Inline Characterization on As-cut Wafers," *Energy Procedia*, 2017.

[2] T. Strauch, M. Demant, P. Krenckel, S. Riepe, and S. Rein, "Analysis of grain structure evolution based on optical measurements of mc-Si wafers," *Sol. Energy Mater. Sol. Cells*, vol. 182, pp. 105–112, 2018, doi: 10.1016/j.solmat.2018.03.009.

[3] A. Kovvali, M. Demant, T. Trötschler, J. Haunschild, and S. Rein, "About the relevance of defect features in as-cut multicrystalline silicon wafers on solar cell performance," in *SiliconPV 2018, the 8th International Conference on Silicon Photovoltaics*, Lausanne, Switzerland, 2018, p. 130011.

[4] T. Strauch, M. Demant, P. Krenckel, S. Riepe, and S. Rein, "Identification of Defect-Supressing Grain Boundaries in Multicrystalline Silicon Based on Measurements of As-Cut Wafers Using Advanced Image Processing," 2017, doi: 10.4229/EUPVSEC20172017-2BO.1.3.

[5] M. Demant *et al.,* "Inline quality rating of multi-crystalline wafers based on photoluminescence images," *Prog. Photovolt: Res. Appl.*, 2015, doi: 10.1002/pip.2706.

[6] T. Trötschler, P. Krenckel, M. Demant, S. Riepe, and S. Rein, "3D Grain Structure and Defect Analysis Based on Optical and PL Measurements of As-Cut-Wafers," in *10th International Workshop on Crystalline Silicon for Solar Cells*, Sendai, Japan, 2018.

[7] Y. Hayama, T. Matsumoto, T. Muramatsu, K. Kutsukake, H. Kudo, and N. Usami, "3D visualization and analysis of dislocation clusters in multicrystalline silicon ingot by approach of data science," *Sol. Energy Mater. Sol. Cells*, vol. 189, pp. 239–244, 2019, doi: 10.1016/j.solmat.2018.06.008.

[8] S. M. Karabanov, O. A. Belyakov, D. V. Suvorov, E. V. Slivkin, A. E. Serebryakov, and A. S. Karabanov, "Study of the Defect Distribution of Multicrystalline Silicon by 3D Visualization of Photoluminescence Signal Images," in *2020 IEEE International Conference on Environment and Electrical Engineering and 2020 IEEE Industrial and Commercial Power Systems Europe (EEEIC / I&CPS Europe)*, Madrid, Spain, Jun. 2020 - Jun. 2020, pp. 1–6.

[9] D. Kohler, D. Kiliani, B. Raabe, S. Seren, and G. Hahn, "Characterization of defect clusters in compensated silicon solar cells," in *26th European Photovoltaic Solar Energy Conference and Exhibition*, Hamburg, 2011, pp. 1–4.

[10] R. Zeidler *et al.,* "Tomographic defect reconstruction of multicrystalline silicon ingots using photoluminescence images of as-cut wafers and solar cells," in *27th EU PVSEC*, Frankfurt, 2012, pp. 636–641.

[11] K. Kutsukake, N. Usami, Y. Ohno, Y. Tokumoto, and I. Yonenaga, "Control of Grain Boundary Propagation in Mono-Like Si: Utilization of Functional Grain Boundaries," *Applied Physics Express*, vol. 6, no. 2, p. 25505, 2013, doi: 10.7567/APEX.6.025505.

[12] S. Riepe *et al.,* "Enhanced Material Quality in SMART Moni-Si Block Cast Ingots by Introduction of Functional Defects," *36th European Photovoltaic Solar Energy Conference and Exhibition, EU PVSEC 2019: Proceedings of the international conference held in Marseille, France, 09-13 September 2019. Marseille, 2019, pp. 120-125*, 2019, doi: 10.4229/EUPVSEC20192019-2AO.5.3.

[13] M. Trempa, C. Reimann, J. Friedrich, G. Müller, and D. Oriwol, "Mono-crystalline growth in directional solidification of silicon with different orientation and splitting of seed crystals," *Journal of Crystal Growth*, vol. 351, pp. 131–140, 2012, doi: 10.1016/j.jcrysgro.2012.04.035.

[14] T. Strauch, M. Demant, P. Krenckel, S. Riepe, and S. Rein, "Analysis of grain structure evolution based on optical measurements of mc Si wafers," *Journal of Crystal Growth*, vol. 454, pp. 147–155, 2016, doi: 10.1016/j.jcrysgro.2016.09.009.

[15] P. Perona and J. Malik, "Scale-space and edge detection using anisotropic diffusion," *IEEE Trans. Pattern Anal. Machine Intell.*, vol. 12, no. 7, pp. 629–639, 1990, doi: 10.1109/34.56205.

[16] A.S. Kovvali, M. Demant, B. Rebba, N. Schüler, J. Haunschild, and S. Rein, "Early Stage Quality Assessment in Silicon Ingots From MDP Brick Characterization," in *37th European Photovoltaic Solar Energy Conference and Exhibition*, online, 2020.

[17] T. Wagner, A. Eckl, R. Koch, and M. Schuetz, "Using Ultra-High Resolution in Brick Transmission Analysis," in *26th European Photovoltaic Solar Energy Conference and Exhibition*, Hamburg, 2011, pp. 2086–2090.

[18] T. Brox, A. Bruhn, N. Papenberg, and J. Weickert, "High Accuracy Optical Flow Estimation Based on a Theory for Warping," in *Lecture Notes in Computer Science, Computer Vision - ECCV 2004*, T. Kanade et al., Eds., Berlin, Heidelberg: Springer-Verlag Berlin Heidelberg, 2004, pp. 25–36.

[19] C. Liu, "Beyond Pixels: Exploring New Representations and Applications for Motion Analysis," Cambridge, MA, USA, 2009.

[20] E. Ilg, N. Mayer, T. Saikia, M. Keuper, A. Dosovitskiy, and T. Brox, "FlowNet 2.0: Evolution of Optical Flow Estimation with Deep Networks," in *IEEE Conference on Computer Vision and Pattern Recognition (CVPR)*, 2017.

[21] W. Schroeder, K. Martin, and B. Lorensen, *The Visualization Toolkit: An object-oriented approach to 3D graphics,* 4th ed. Clifton Park, NY: Kitware, 2006.

[22] P. Ramachandran and G. Varoquaux, "Mayavi: 3D Visualization of Scientific Data," *Computing in Science & Engineering*, vol. 13, no. 2, pp. 40–51, 2011.

[23] M. Trempa *et al.,* "Defect formation induced by seed-joints during directional solidification of quasi-mono-crystalline silicon ingots," *Journal of Crystal Growth*, vol. 405, no. 0, pp. 131–141, 2014, doi: 10.1016/j.jcrysgro.2014.08.002.